

**SELF-SUPERVISED LEARNING FOR A NONLINEAR INVERSE  
PROBLEM WITH FORWARD OPERATOR INVOLVING AN  
UNKNOWN FUNCTION ARISING IN PHOTOACOUSTIC  
TOMOGRAPHY**

Gyeongha Hwang<sup>1</sup>, Gihyeon Jeon<sup>2\*</sup>, Sunghwan Moon<sup>3</sup>

<sup>1</sup> Department of Mathematics, Yeungnam University, Gyeongsan 38541, Republic of Korea

<sup>2</sup> School of Mathematics, Kyungpook National University, Daegu 41566, Republic of Korea

<sup>3</sup> Department of Mathematics, Kyungpook National University, Daegu 41566, Republic of Korea

\*Corresponding author E-mails: rydbr6709@knu.ac.kr

**ABSTRACT.** In this article, we concern with a nonlinear inverse problem with forward operator involving an unknown function. The problem arises in diverse applications and is challenging by the presence of the unknown function, which makes it ill-posed. Additionally, the nonlinear nature of the problem makes it difficult to use traditional methods and thus the study has addressed a simplified version of the problem by either linearizing it or assuming knowledge of the unknown function. Here, we propose a self-supervised learning to directly tackle a nonlinear inverse problem involving an unknown function. In particular, we focus on an inverse problem derived in Photoacoustic Tomography (PAT) which is a hybrid medical imaging with high resolution and contrast. PAT can be modelled based on the wave equation. The measured data is the solution of the equation restricted to the surface and the initial pressure of the equation contains the biological information on the object of interest. The speed of sound wave in the equation is unknown. Our goal is to determine the initial pressure and the speed of sound wave simultaneously. Under a simple assumption that the sound speed is a function of the initial pressure, the problem becomes a nonlinear inverse problem involving an unknown function. The experimental results demonstrate that the proposed algorithm performs successfully.

## 1 Introduction

Inverse problem is to find the cause factor from the observed data, which has applications in many fields such as optics, radar, acoustics, communication theory, signal processing, medical imaging, computer vision, geophysics, oceanography, and astronomy because it tells us about what we cannot directly observe. The forward operator, the inverse of the inverse problem, can be modelled as an (non)-linear system and often involves an unknown function. Due to the nature of the inverse problem, it is usually very hard to know the cause factor. For example, in medical imaging the cause factor is the human body section and in seismology, we never know the structure of the earth's interior.

In this article, we concern with a nonlinear inverse problem with forward operator involving an unknown function. Our goal is to find the unknown function and the inverse operator simultaneously from the measurements. The problem is generally ill-posed because of

the unknown function. Additionally, the nonlinearity in the problem makes conventional methods difficult to use. To handle the problem, one may simplify the problem linearly or assume knowledge of the unknown function. Here we propose a self-supervised framework to directly tackle a nonlinear inverse problem involving an unknown function. In particular, we address an inverse problem derived in Photoacoustic Tomography (PAT). Although our proposed framework has been proposed to solve the problem arising in PAT, it is generic and can be extended to handle a nonlinear inverse problem involving an unknown function.

The rest of the section is devoted to an introduction of PAT. In section 2, we formulate an inverse problem arising in PAT, which is nonlinear and also involves an unknown function. The structure and learning method of the proposed framework for the problem are described in section 3. The numerical simulation results in section 4 demonstrate that the proposed algorithm performs successfully.

## 1.1 Photoacoustic Tomography

PAT is a hybrid medical imaging that combines the high contrast of optical imaging with the high spatial resolution of ultrasound images [1, 2, 3]. The physical basis of PAT is the photoacoustic effect discovered by Bell in 1881 [4]. In PAT, when a non-destructive testing target object absorbs a non-ionizing laser pulse, it thermally expands and emits acoustic waves. The emitted ultrasound contains biological information on the target object and is measured by a detector placed around it. The internal image of the target object is reconstructed from this measured data. The advantage of PAT is that it is economical and less harmful because of non-ionizing radiation use [5].

The propagation of the emitted ultrasound  $p(\mathbf{x}, t)$  can be described by the wave equation

$$\partial_t^2 p(\mathbf{x}, t) = c(\mathbf{x})^2 \Delta_{\mathbf{x}} p(\mathbf{x}, t) \quad \text{on } \mathbb{R}^2 \times [0, \infty) \quad (1)$$

with the initial conditions

$$p(\mathbf{x}, 0) = f(\mathbf{x}) \quad \partial_t p(\mathbf{x}, 0) = 0 \quad \text{on } \mathbb{R}^2. \quad (2)$$

Here  $c$  is the speed of waves and  $f$  is the initial pressure which contains biological information such as the location of a cancer cells in a physically small tissue. It is natural assumption that  $f$  has compact support in the bounded domain  $\Omega$  and the detectors are located on the boundary  $\partial\Omega$  of the domain. Regarding the measurement procedure, the point-shaped detector measures the average pressure above  $\partial\Omega$  where the detectors are located and this average pressure is the value of a pressure wave  $p(\mathbf{x}, t)$ . Therefore, one of mathematical problems in PAT is reconstructing  $f$  from the measured data  $p|_{\partial\Omega \times [0, \infty)}$ , which implies obtaining an internal image of the target object.

It is well-known that given the initial pressure  $f$  and the speed  $c$ , the solution  $p$  is determined uniquely. Let us define the wave forward operator  $\mathcal{W}$  as

$$\mathcal{W} : (f, c) \mapsto p|_{\partial\Omega \times [0, \infty)}, \quad \text{i.e.,} \quad \mathcal{W}(f, c) = p|_{\partial\Omega \times [0, \infty)}.$$

Reconstructing problem for  $f$  from  $\mathcal{W}(f, c)$  is studied when speed  $c$  is constant [6, 7]. Okanen, Stefanov and Uhlmann study the explicit reconstruction when the sound speed

is known [8, 9]. If  $c$  depends on space variable  $\mathbf{x}$ , the problem become much more difficult. A few of researchers have studied the problem with a given variable sound speed [10, 11, 12, 13]. Liu and Uhlmann figure out the sufficient conditions for recovering  $f$  and  $c$  [14].

Recently, the application of deep learning in an medical imaging including PAT has been investigated extensively. Roles of deep learning in tomography include forward and inverse operator approximation, image reconstruction from sparse data, and artifact/noise removal from reconstructed images [15, 16, 17, 18, 19, 20, 21]. There are also studies on limited-view data (see [22, 23]). H. Shan et al. propose an iterative optimization algorithm which reconstructs  $f$  and  $c$  simultaneously via a supervised learning [24]. However, most works deal with linear inverse problems or inverse problems without involving an unknown function [25].

Many studies on PAT with deep learning are based on a supervised learning. A supervised learning exploits a collection of paired data of the boundary data and the initial pressure. In practical applications, it is difficult to obtain the initial pressure, because initial pressure represents internal human body. Therefore, it is necessary to study a learning method exploiting the boundary data only. One such method is a self-supervised learning which exploits supervised signals that are generated from the input data by leveraging its structure [26, 27].

## 2 Problem formulation

In this section, we formulate the problem precisely. For this, we will make several assumptions. First we assume  $f$  has compact support, since a target object is finite. Secondly,  $c$  is assumed to be a function of  $f$ , namely  $c(\mathbf{x})^2 = \Gamma(f(\mathbf{x}))$  for some function  $\Gamma : [0, 1] \rightarrow [0, \infty)$ , because the wave speed  $c$  depends on the medium. Lastly, we assume that  $\Gamma(0)$  and  $\Gamma(1)$  are known, namely  $\Gamma(0) = c_0$  and  $\Gamma(1) = c_1$ . The last assumption is reasonable because  $\Gamma(0)$  and  $\Gamma(1)$  represent the wave speeds in the air and the highest thermal expansion coefficient respectively. Then the equation (1) is rewritten as:

$$\partial_t^2 p(\mathbf{x}, t) = \Gamma(f(\mathbf{x})) \Delta_{\mathbf{x}} p(\mathbf{x}, t) \quad \text{on } \mathbb{R}^2 \times [0, \infty). \quad (3)$$

Let us define  $\mathcal{W}_\Gamma$  by  $\mathcal{W}_\Gamma(f) = p|_{\partial\Omega \times [0, \infty)}$  where  $p$  is the solution of (3) with initial conditions (2). Then the inverse problem can be formulated as determining unknown  $\Gamma$  and  $f$  from a given  $\mathcal{W}_\Gamma(f)$ . However, this problem is ill-posed: for any  $\Gamma'$  satisfying

$$\begin{cases} \Gamma = \Gamma' \text{ on } \text{Im}(f) \\ \Gamma \neq \Gamma' \text{ on } \text{Dom}(\Gamma) \setminus \text{Im}(f), \end{cases}$$

we have  $\mathcal{W}_\Gamma(f) = \mathcal{W}_{\Gamma'}(f)$ . Hence  $\Gamma$  can not be uniquely determined from  $\mathcal{W}_\Gamma(f)$ . There is also a possibility that there exist  $\Gamma_1, \Gamma_2, f_1$  and  $f_2$  such that  $\Gamma_1 \neq \Gamma_2$ ,  $f_1 \neq f_2$  and  $\mathcal{W}_{\Gamma_1}(f_1) = \mathcal{W}_{\Gamma_2}(f_2)$ . Instead, we consider the following inverse problem:

**Problem 1.** *Let the collection of boundary data  $\mathcal{B}_\Gamma := \{\mathcal{W}_\Gamma(f) \mid \Gamma : [0, 1] \rightarrow [0, \infty), \Gamma(0) = c_0, \Gamma(1) = c_1 \text{ and } f \in L^2(\mathbb{R}^2) \text{ has compact support}\}$  be given.*

1. Determine unknown  $\Gamma$  from  $\mathcal{B}_\Gamma$ .
2. For all  $\mathcal{W}_\Gamma(f) \in \mathcal{B}_\Gamma$ , determine  $f$ .

Then the uniqueness statements for Problem 1 are

**Hypothesis 1.** If  $\Gamma_1 \neq \Gamma_2$ , then  $\mathcal{B}_{\Gamma_1} \neq \mathcal{B}_{\Gamma_2}$ .

and

**Hypothesis 2.** For fixed  $\Gamma$ , if  $f_1 \neq f_2$ , then  $\mathcal{W}_\Gamma(f_1) \neq \mathcal{W}_\Gamma(f_2)$ .

In this article, we aim to solve Problem 1 under Hypothesis 1 and 2. The problem is difficult to solve because of

1. (3) involves unknown  $\Gamma$ .
2. (3) is not linear.

We are going to solve Problem 1 by exploiting a deep neural network (DNN). Since DNN can only handle with finite data, we address the following inverse problem.

**Problem 2.** For given  $\{\mathcal{W}_\Gamma(f_i) \mid \Gamma : [0, 1] \rightarrow [0, \infty), \Gamma(0) = c_0, \Gamma(1) = c_1 \text{ and } f_i \in L^2(\mathbb{R}^2) \text{ has compact support, } i = 1, \dots, N\}$ , determine  $\Gamma$  and  $\{f_i \mid i = 1, \dots, N\}$ .

### 3 Network Design

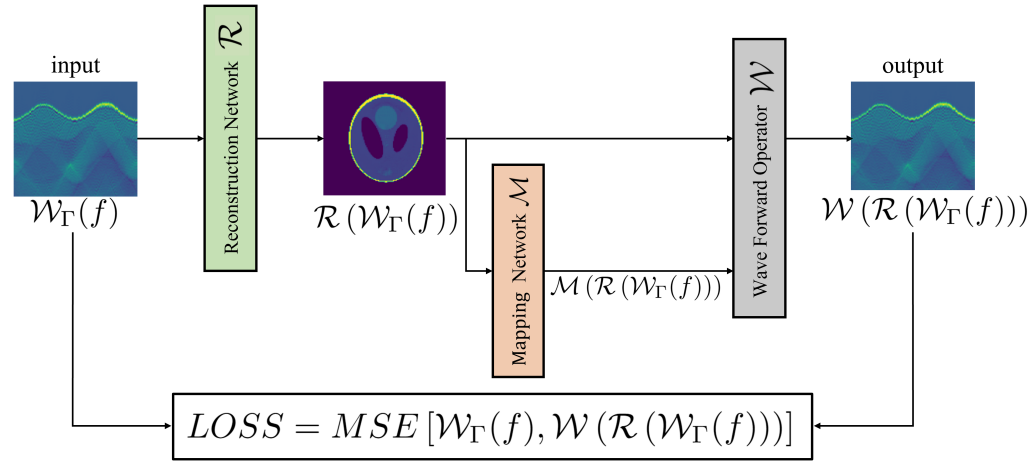


Figure 1: The network architecture

We propose a self-supervised learning for the problem formulated in section 2. Our goal is simultaneously reconstructing  $\{f_i\}_{i=1}^N$  and  $\Gamma$  from given collection  $\{\mathcal{W}_\Gamma(f_i)\}_{i=1}^N$ . The proposed framework is depicted in Figure 1. It consists of three components:

1. Reconstruction network  $\mathcal{R}$
2. Mapping network  $\mathcal{M}$
3. Wave forward operator  $\mathcal{W}$ .

The reconstruction network  $\mathcal{R}$  learns to reconstruct the initial data from the measured data. The mapping network  $\mathcal{M}$  approximates the function  $\Gamma : [0, 1] \rightarrow [0, \infty)$  satisfying  $c(\mathbf{x})^2 = \Gamma(f(\mathbf{x}))$ . The forward operator  $\mathcal{W}$  assigns to the initial data and the wave speed the measured data. Here we adopt the  $k$ -space method. If every component in the framework functions properly, then output should be same to the input. Thus we define the loss function as the difference between the input and the output:

$$\mathcal{L} = \frac{1}{N} \sum_{i=1}^N \frac{\|\mathcal{W}_\Gamma(f_i) - \mathcal{W}_\mathcal{M}(\mathcal{R}(\mathcal{W}_\Gamma(f_i)))\|_2}{\|\mathcal{W}_\Gamma(f_i)\|_2}.$$

**Remark.** *Our method estimates  $\Gamma$  and the inverse operator  $\mathcal{W}_\Gamma^{-1}$ . The estimated inverse operator can be used for the fast inference of the initial pressure from the boundary measurement.*

**Remark.** *The proposed framework is generic and can be extended to handle a nonlinear inverse problem involving an unknown function.*

Now, the detailed structures of each component in the framework are described below.

### 3.1 Reconstruction network $\mathcal{R}$

The reconstruction network  $\mathcal{R}$  is a network that reconstruct  $f$  from input data  $\mathcal{W}_\Gamma(f)$ . Indeed, it approximates the inverse map  $\mathcal{W}_\Gamma^{-1} : \mathcal{W}_\Gamma(f) \mapsto f$ . If the speed  $\Gamma$  of the wave is constant, it is well-known that the inverse map of (3) is linear [7, 28, 29]. Inspired by this fact, we propose the reconstruction network as a perturbation of a linear map:

$$\mathcal{R} := T_1 + U \circ T_2, \quad (4)$$

where  $T_1, T_2 : \mathbb{R}^{m \times m} \rightarrow \mathbb{R}^{m \times m}$  are linear and  $U : \mathbb{R}^{m \times m} \rightarrow \mathbb{R}^{m \times m}$  is the U-net described in Figure 2. U-net is a type of convolutional neural network (CNN) introduced in [30] and is used widely in medical imaging. U-net consists of a contracting path and an expansive path. The contacting path has a typical CNN structure, where the input data is extracted into feature map with small size and large channel. In the expansive path, the size of the feature map increases again, and the number of channels decreases. In the end of  $\mathcal{R}$ , since the range of  $f$  is  $[0, 1]$ , we used the clamp function which rounds up values smaller than the minimum and round down values larger than the maximum.

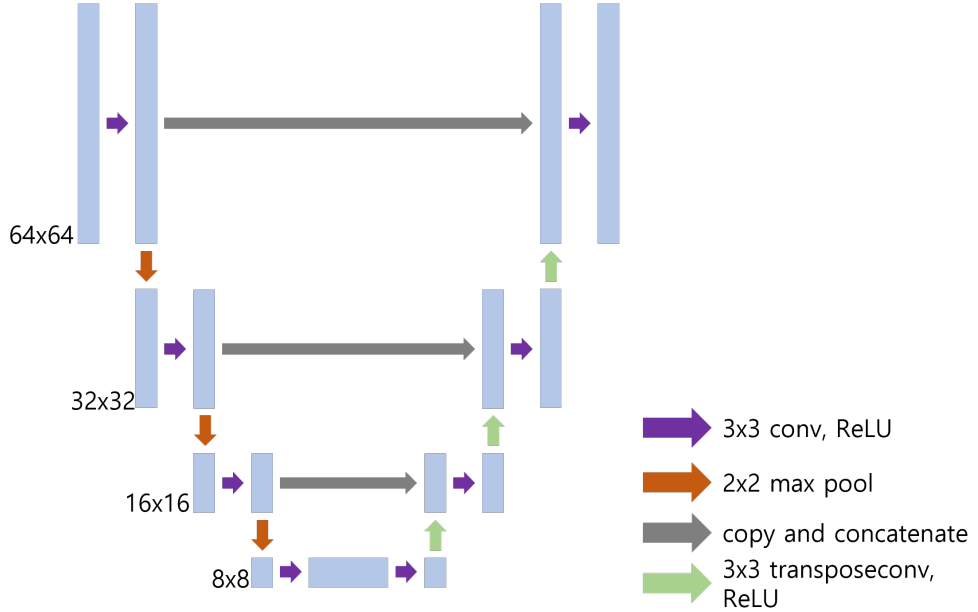


Figure 2: U-net architecture for  $64 \times 64$  size

The proposed reconstruction network show a high performance for the low resolution data like  $64 \times 64$  (see section 4.3.1). In case of high resolution data, however the linear operators  $T_1$  and  $T_2$  in the reconstruction network  $\mathcal{R}$  make some problems, because they contains too many parameters. It causes lots of critical points which impede the convergence to the global minimum. It also makes a hardware issue and thus for the high resolution data, we employ Pixel Shuffle and Pixel Unshuffle which reduce the number of parameters contained in linear operators [31]. The Pixel Unshuffle splits one image into several images and the Pixel Shuffle merges several images into one image, as illustrated in Figure 3. Instead of applying the linear operators ( $T_1$  and  $T_2$ ) directly to the high resolution data, we process the data as follows (see Figure 4) :

1. Split the high resolution data  $(m \times m)$  into four low resolution data  $(\frac{m}{2} \times \frac{m}{2})$  by exploiting the Pixel Unshuffle.
2. Apply four different linear operators to each low resolution data.
3. Merge the outputs of the linear operators by using the Pixel Shuffle.

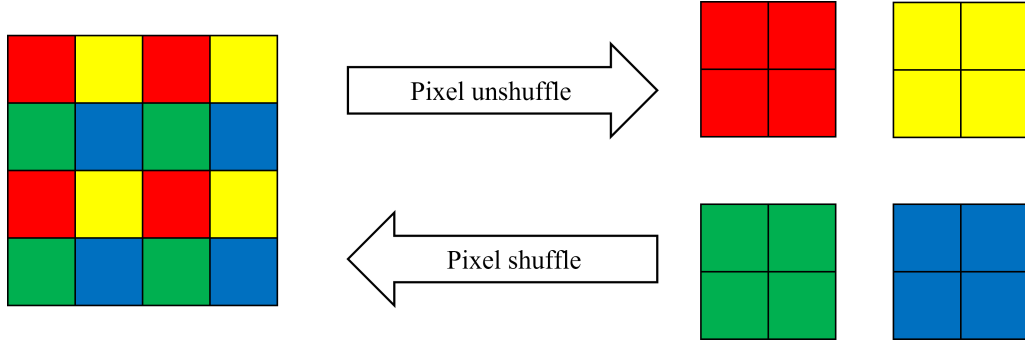


Figure 3: Pixel Shuffle and Pixel Unshuffle

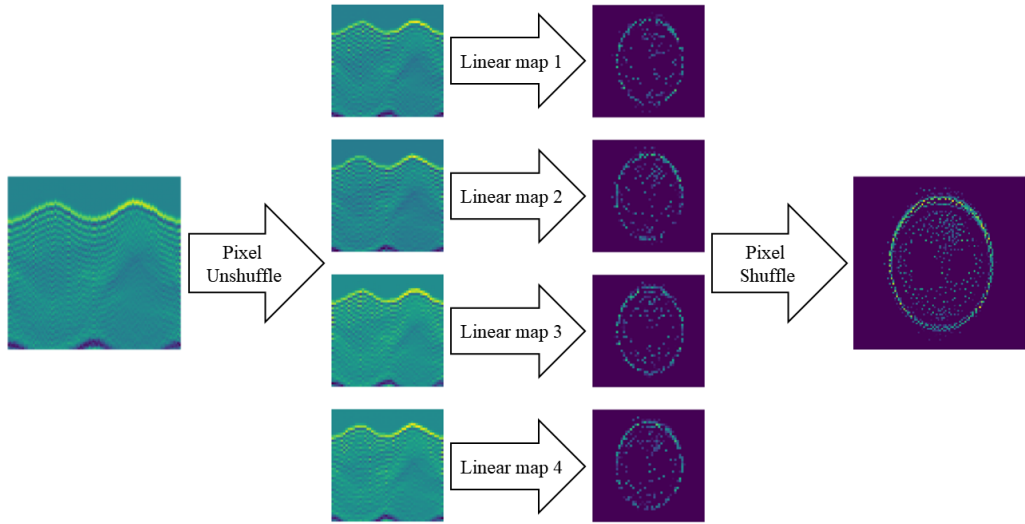


Figure 4: Architecture of alternative map to linear for high resolution data

### 3.2 Mapping network $\mathcal{M}$

We use multilayer perceptron (MLP) to approximate unknown  $\Gamma$ , because MLP can approximate any continuous function (a universal approximation theorem, see [32, 33]). The proposed network is a simple structure containing only three hidden layers of 10 nodes. To satisfy the assumption that  $\Gamma(0) = c_0$  and  $\Gamma(1) = c_1$ , the output of MLP is slightly manipulated as

$$\mathcal{M}(f) = \text{MLP}(f) - \text{MLP}(0) * (1 - f) - \text{MLP}(1) * f + ((c_1 - c_0)f + c_0),$$

so that

$$\mathcal{M}(0) = c_0 \text{ and } \mathcal{M}(1) = c_1. \quad (5)$$

### 3.3 Forward problem

A solution of the initial value problem (3) can be computed by the  $k$ -space method [34, 35]. The  $k$ -space method is a numerical method for computing solution of acoustic wave propagation, which uses information in the frequency space to obtain a solution for the next time step. For calculating propagation of  $p(\mathbf{x}, t)$ , let  $w(\mathbf{x}, t) = \frac{1}{\Gamma(f(\mathbf{x}))} p(\mathbf{x}, t)$  be an auxiliary field. Then we have,

$$\partial_t^2 w(\mathbf{x}, t) = \Delta_{\mathbf{x}} [\Gamma(f(\mathbf{x})) w(\mathbf{x}, t)].$$

Taking the Fourier transform  $\mathcal{F}_{\mathbf{x}}$  for  $w$  with respect to  $\mathbf{x}$  yields

$$\partial_t^2 \mathcal{F}_{\mathbf{x}} w(\mathbf{k}, t) = -|\mathbf{k}|^2 \mathcal{F}_{\mathbf{x}} [\Gamma(f(\cdot)) w(\cdot, t)](\mathbf{k}). \quad (6)$$

Meanwhile, the numerical approximation of the second derivative of  $\mathcal{F}_{\mathbf{x}} w$  is

$$\partial_t^2 \mathcal{F}_{\mathbf{x}} w(\mathbf{k}, t) \approx \frac{\mathcal{F}_{\mathbf{x}} w(\mathbf{k}, t + \Delta t) - 2\mathcal{F}_{\mathbf{x}} w(\mathbf{k}, t) + \mathcal{F}_{\mathbf{x}} w(\mathbf{k}, t - \Delta t)}{(\Delta t)^2}, \quad (7)$$

where  $\Delta t$  is the time step. Then, by combining (6) and (7), we have

$$\mathcal{F}_{\mathbf{x}} w(\mathbf{k}, t + \Delta t) = 2\mathcal{F}_{\mathbf{x}} w(\mathbf{k}, t) - \mathcal{F}_{\mathbf{x}} w(\mathbf{k}, t - \Delta t) - (\Delta t)^2 |\mathbf{k}|^2 \mathcal{F}_{\mathbf{x}} [\Gamma(f(\cdot)) w(\cdot, t)](\mathbf{k}).$$

By taking the inverse Fourier transform  $\mathcal{F}_{\mathbf{k}}^{-1}$ , we obtain

$$w(\mathbf{x}, t + \Delta t) = 2w(\mathbf{x}, t) - w(\mathbf{x}, t - \Delta t) - \mathcal{F}_{\mathbf{k}}^{-1} \left[ (\Delta t)^2 |\cdot|^2 \mathcal{F}_{\mathbf{x}} [\Gamma(f) w](\cdot, t) \right] (\mathbf{x}).$$

Here, replacing  $(\Delta t)^2 |\mathbf{k}|^2$  in the third term with  $4 \sin^2 \left( \frac{(\Delta t)|\mathbf{k}|}{2} \right)$  provides more accurate discretization (see [34, 35]). Finally, we have wave propagation formula:

$$w(\mathbf{x}, t + \Delta t) = 2w(\mathbf{x}, t) - w(\mathbf{x}, t - \Delta t) - \mathcal{F}_{\mathbf{k}}^{-1} \left[ 4 \sin^2 \left( \frac{(\Delta t)|\cdot|}{2} \right) \mathcal{F}_{\mathbf{x}} [\Gamma(f) w](\cdot, t) \right] (\mathbf{x}),$$

or equivalently,

$$p(\mathbf{x}, t + \Delta t) = 2p(\mathbf{x}, t) - p(\mathbf{x}, t - \Delta t) - \Gamma(f) \mathcal{F}_{\mathbf{k}}^{-1} \left[ 4 \sin^2 \left( \frac{(\Delta t)|\cdot|}{2} \right) \mathcal{F}_{\mathbf{x}} [p](\cdot, t) \right] (\mathbf{x}).$$

## 4 Numerical Simulations

In this section, we present the details of implementation and experimental results when  $\Omega$  is the unit ball.

## 4.1 Datasets

The Shepp-Logan phantom, an artificial image that describes a cross section of the brain commonly used for simulation in tomography, contains 10 ellipses [36]. Each ellipse is created with 6 parameters: major axis, minor axis, the  $x$ -coordinate and the  $y$ -coordinate of center, rotation angle, and intensity value. The data set of the initial condition  $f$  defined on  $[-1.0, 1.0]^2 \subset \mathbb{R}^2$  is generated by slightly changing these 6 parameters with

$$\text{supp}(f) \subset \left\{ (x, y) \in \mathbb{R}^2 : \frac{x^2}{0.69^2} + \frac{y^2}{0.92^2} \leq 1 \right\}.$$

We create a set of 2,688 phantoms  $P = \{f_i\}_{i=1}^{2688}$ . For  $\Gamma$ , we consider four cases: linear, square root, square, and constant

1.  $\Gamma_1(f) = 0.3f + 0.7$
2.  $\Gamma_2(f) = 0.3\sqrt{f} + 0.7$
3.  $\Gamma_3(f) = 0.3f^2 + 0.7$
4.  $\Gamma_4(f) = 0.7$ .

For  $1 \leq j \leq 4$ , we make the collection of data  $\{\mathcal{W}_{\Gamma_j} f_i\}_{i=1}^{2688}$  by using the forward operator for  $P$  and  $\Gamma_j$ . Of the 2,688 data, we use 2,048 data for training, 128 data for validation and 512 data for testing respectively.

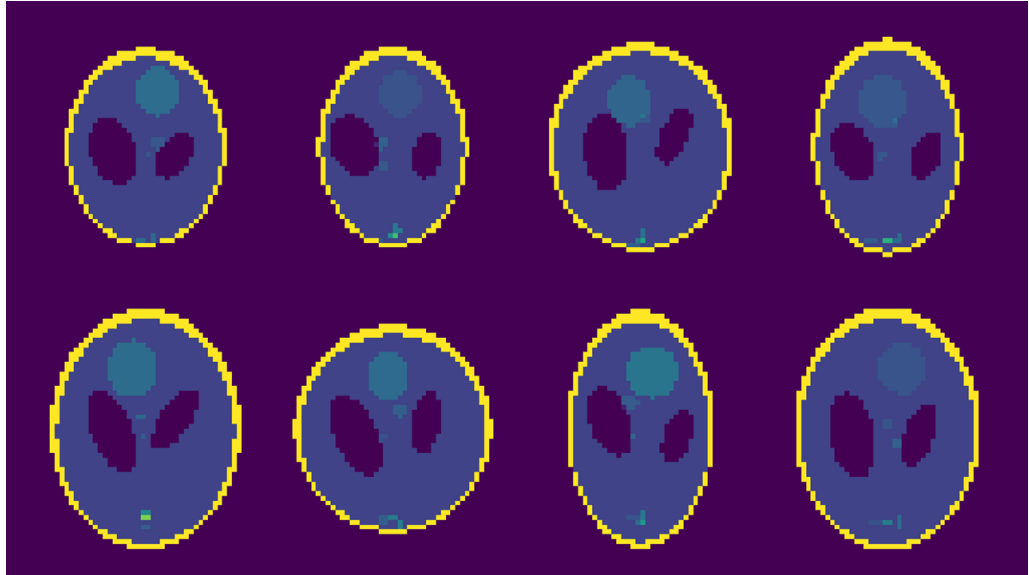


Figure 5: Examples of phantoms

## 4.2 Training

We use the Adam optimizer based on stochastic gradient descent and adaptive moment estimation to train the network [37]. There are two neural networks in the proposed frameworks: the reconstruction network  $\mathcal{R}$  and the mapping network  $\mathcal{M}$ . The learning rates for linear term of  $\mathcal{R}$ , perturbation term of  $\mathcal{R}$ , and  $\mathcal{M}$  are chosen to be  $10^{-4}$ ,  $10^{-3}$ , and  $10^{-3}$ , respectively. Momentum parameters of the Adam optimizer were set at  $\beta_1 = 0.9$  and  $\beta_2 = 0.999$ , respectively.

We specifically put the batch size to 2. For general tasks, a moderately large batch size reduces training time. However, in this problem, a small batch size is advantageous because our model must be able to reconstruct an exact image for each data rather than an average result.

## 4.3 Results

In this section, we illustrate experimental results. The overall results are displayed in Figure 6, Table 1, Figure 7, Figure 8, Table 2 and Figure 9. Here the losses for  $f$  and  $\mathcal{W}_\Gamma(f)$  are respectively defined by

$$\text{loss for } f = \frac{1}{N} \sum_{i=1}^N \frac{\|f_i - \mathcal{R}(\mathcal{W}_\Gamma(f_i))\|_2}{\|f_i\|_2},$$

and

$$\text{loss for } \mathcal{W}_\Gamma f = \frac{1}{N} \sum_{i=1}^N \frac{\|\mathcal{W}_\Gamma(f_i) - \mathcal{W}_\mathcal{M}(\mathcal{R}(\mathcal{W}_\Gamma(f_i)))\|_2}{\|\mathcal{W}_\Gamma(f_i)\|_2}.$$

### 4.3.1 Low resolution data

We conduct the simulation utilizing a dataset of images with a size of  $64 \times 64$ . The results for the mapping networks are shown in Figure 6. We see that the mapping networks accurately approximates  $\Gamma$ . When  $\Gamma_3 = 0.3f^2 + 0.7$ , there is a difference between the plot of the mapping network  $\mathcal{M}$  and the plot of  $\Gamma$ . This is because the values of  $f \in P$  almost belong to  $[0, 0.3] \cup 1$  and so it has little effect on  $\mathcal{W}_\Gamma(f)$ . In all cases, the process of training the mapping networks requires approximately  $10^3$  iterations. The results of the reconstruction networks are illustrated in Table 1 and Figure 7. Table 1 shows the test errors. So it can be concluded that the reconstruction networks accurately approximate the inverse maps in each case. The training of the reconstruction networks necessitates approximately  $10^5$  iterations.

**Remark.** *The assumption on  $\Gamma$ , (5) is crucial. If constraint (5) is not given in  $\mathcal{M}$ , it may take a long time to approximate  $\Gamma$ , or it may fail to find  $\Gamma$ . Under the constraint,  $\mathcal{M}$  can quickly determine  $\Gamma$ . Early determination of  $\Gamma$  helps the learning of reconstruction networks.*

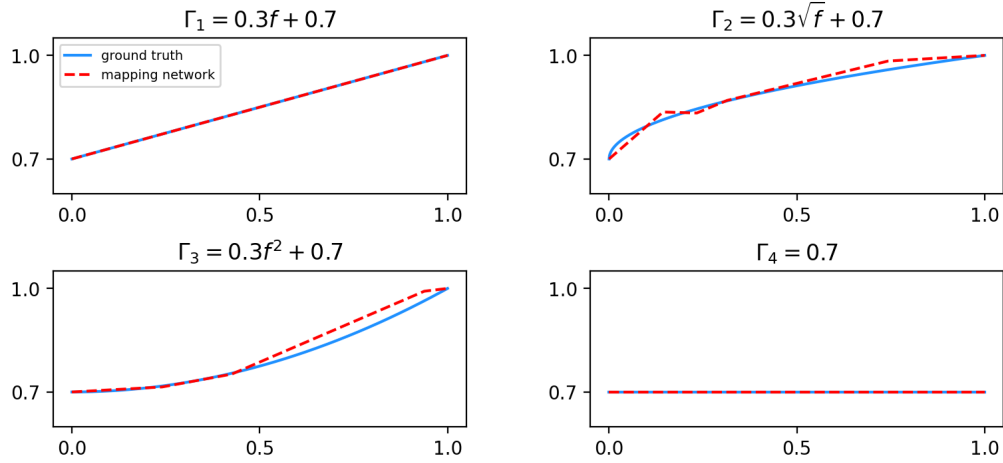


Figure 6: Comparison of the mapping network  $\mathcal{M}$  and ground truth  $\Gamma$  for  $64 \times 64$  data

Assumption	loss for $f$	loss for $\mathcal{W}_\Gamma(f)$
$\Gamma_1 = 0.3f + 0.7$	0.00504	0.00702
$\Gamma_2 = 0.3\sqrt{f} + 0.7$	0.00537	0.00947
$\Gamma_3 = 0.3f^2 + 0.7$	0.00557	0.00634
$\Gamma_4 = 0.7$	0.01373	0.00456

Table 1: Test errors for  $f$  and  $\mathcal{W}_\Gamma(f)$  according to  $\Gamma$  after 102,400 iterations for  $64 \times 64$  data

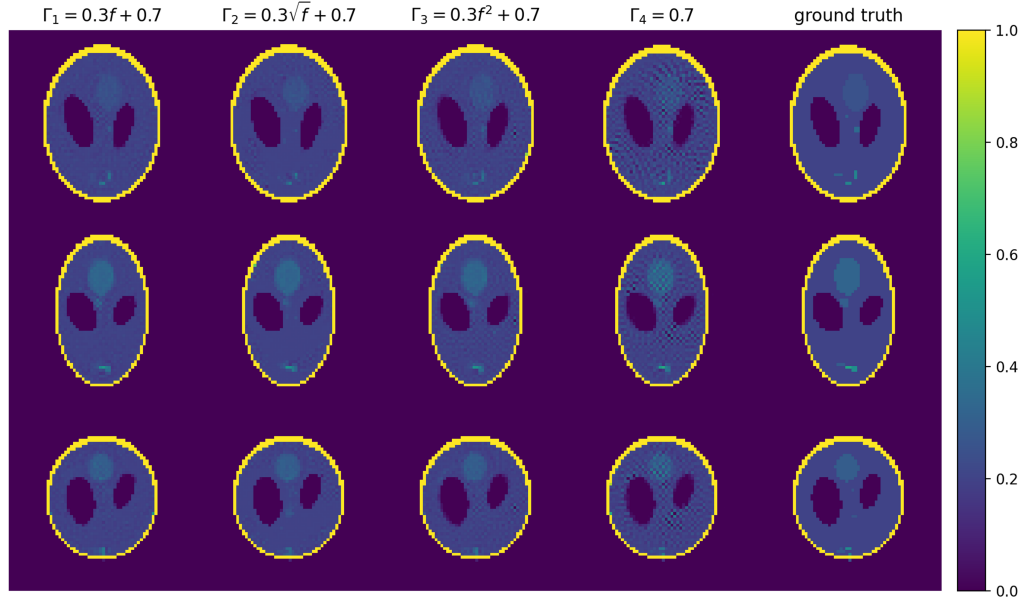


Figure 7: Reconstruction results according to  $\Gamma$  for  $64 \times 64$  data

#### 4.3.2 High resolution data

In the simulation for high resolution data, two linear operators  $T_1$  and  $T_2$  in the reconstruction network (4) are replaced by alternative map described in Figure 4. The dataset is prepared with images of a size of  $96 \times 96$ . Similarly to the low resolution case, the mapping network  $\mathcal{M}$  approximates  $\Gamma$  accurately within  $10^3$  iterations (Figure 8). On the other hand, the reconstruction networks for each  $\Gamma$  exhibit a slight decrease in performance but still acceptable (Table 2 and Figure 9). We surmise that the slight decrease in performance is a result of the reduction in parameters brought about by the Pixel Unshuffle and Pixel Shuffle operations.

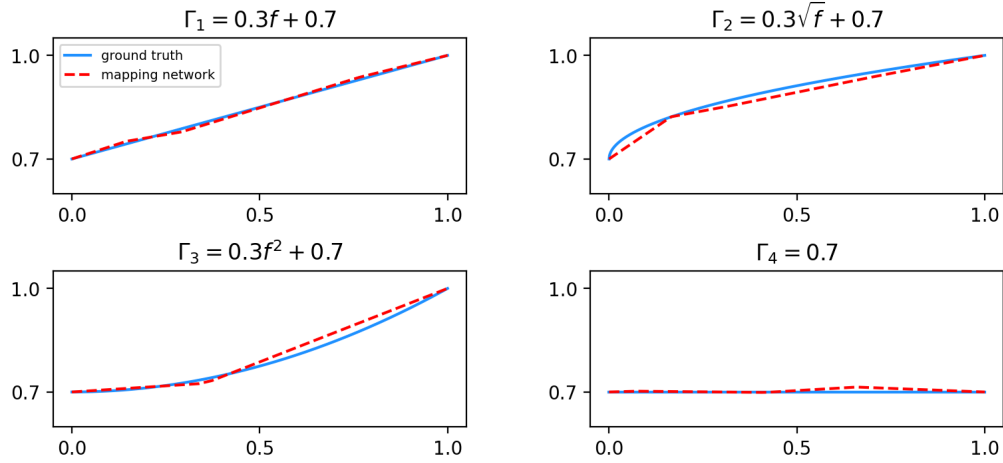


Figure 8: Comparison of the mapping network  $\mathcal{M}$  and ground truth  $\Gamma$  for  $96 \times 96$  data

Assumption	loss for $f$	loss for $\mathcal{W}_\Gamma(f)$
$\Gamma_1 = 0.3f + 0.7$	0.00860	0.01293
$\Gamma_2 = 0.3\sqrt{f} + 0.7$	0.01023	0.01679
$\Gamma_3 = 0.3f^2 + 0.7$	0.00710	0.01132
$\Gamma_4 = 0.7$	0.00689	0.69511

Table 2: Test errors for  $f$  and  $\mathcal{W}_\Gamma(f)$  according to  $\Gamma$  after 102,400 iterations for  $96 \times 96$  data

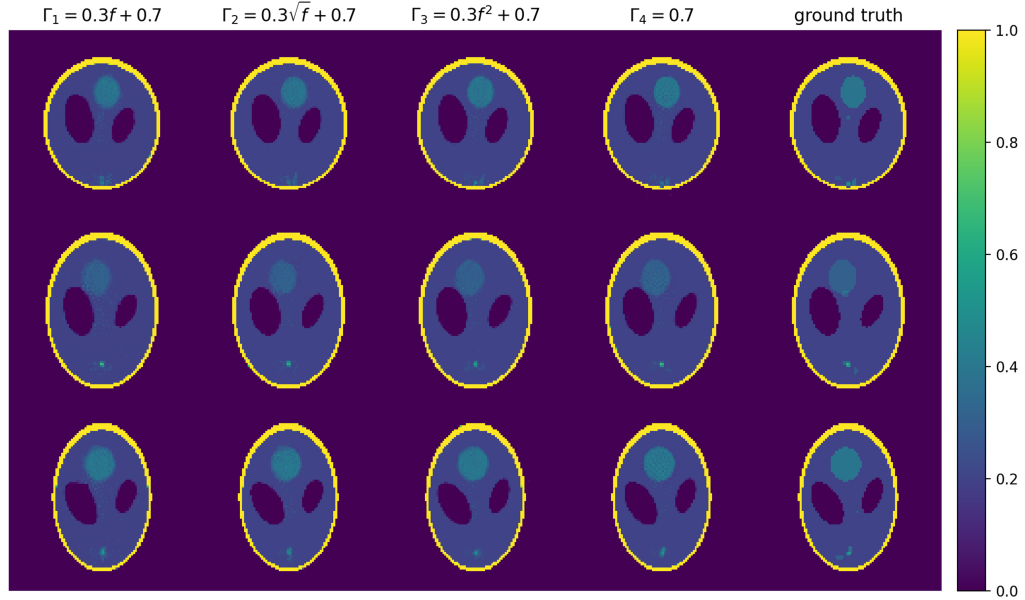


Figure 9: Reconstruction results according to  $\Gamma$  for  $96 \times 96$  data

## 5 Conclusions

Here, we propose a self-supervised learning for a nonlinear inverse problem with forward operator involving an unknown function. In medical imaging such as PAT, the initial pressure is mostly untrackable for the measured data. Moreover it is difficult to know the wave speed. So it is necessary to reconstruct the initial pressure  $f$  and the wave speed simultaneously. Under the simple assumption, the problem becomes a nonlinear inverse problem involving an unknown function. The experimental results demonstrate the high performance of the proposed algorithm. Our framework can be extended to a nonlinear inverse problem involving an unknown function, formulated under more complicated situations. This can be an interesting line of future research.

## References

- [1] Huabei Jiang. Photoacoustic tomography. CRC Press, 2018.
- [2] Jun Xia, Junjie Yao, and Lihong V Wang. Photoacoustic tomography: principles and advances. Electromagnetic waves (Cambridge, Mass.), 147:1, 2014.
- [3] Peter Kuchment. The Radon transform and medical imaging. SIAM, 2013.

- [4] Alexander Graham Bell. On the production and reproduction of sound by light. In *Proc. Am. Assoc. Adv. Sci.*, volume 29, pages 115–136, 1881.
- [5] Idan Steinberg, David M Huland, Ophir Vermesh, Hadas E Frostig, Willemieke S Tummers, and Sanjiv S Gambhir. Photoacoustic clinical imaging. *Photoacoustics*, 14:77–98, 2019.
- [6] Gerhard Zangerl, Sunghwan Moon, and Markus Haltmeier. Photoacoustic tomography with direction dependent data: An exact series reconstruction approach. *Inverse Problems*, 35(11):114005, 2019.
- [7] Minghua Xu and Lihong V Wang. Universal back-projection algorithm for photoacoustic computed tomography. *Physical Review E*, 71(1):016706, 2005.
- [8] Lauri Oksanen and Gunther Uhlmann. Photoacoustic and thermoacoustic tomography with an uncertain wave speed. *Mathematical Research Letters*, 2014.
- [9] Plamen Stefanov and Gunther Uhlmann. Thermoacoustic tomography with variable sound speed *Inverse Problems*, 25(7):075011, 16, 2009.
- [10] Jianliang Qian, Plamen Stefanov, Gunther Uhlmann, and Hongkai Zhao. An efficient neumann series–based algorithm for thermoacoustic and photoacoustic tomography with variable sound speed. *SIAM Journal on Imaging Sciences*, 4(3):850–883, 2011.
- [11] Zakaria Belhachmi, Thomas Glatz, and Otmar Scherzer. A direct method for photoacoustic tomography with inhomogeneous sound speed. *Inverse Problems*, 32(4):045005, 2016.
- [12] Yulia Hristova, Peter Kuchment, and Linh Nguyen. Reconstruction and time reversal in thermoacoustic tomography in acoustically homogeneous and inhomogeneous media. *Inverse problems*, 24(5):055006, 2008.
- [13] Minam Moon, Injo Hur, and Sunghwan Moon. Singular value decomposition of the wave forward operator with radial variable coefficients. *arXiv preprint arXiv:2208.10793*, 2022.
- [14] Hongyu Liu and Gunther Uhlmann. Determining both sound speed and internal source in thermo-and photo-acoustic tomography. *Inverse Problems*, 31(10):105005, 2015.
- [15] Stephan Antholzer, Markus Haltmeier, Robert Nuster, and Johannes Schwab. Photoacoustic image reconstruction via deep learning. In *Photons Plus Ultrasound: Imaging and Sensing 2018*, volume 10494, pages 433–442. SPIE, 2018.
- [16] Gregory Ongie, Ajil Jalal, Christopher A Metzler, Richard G Baraniuk, Alexandros G Dimakis, and Rebecca Willett. Deep learning techniques for inverse problems in imaging. *IEEE Journal on Selected Areas in Information Theory*, 1(1):39–56, 2020.
- [17] Ge Wang, Jong Chul Ye, and Bruno De Man. Deep learning for tomographic image reconstruction. *Nature Machine Intelligence*, 2(12):737–748, 2020.

- [18] Janek Gröhl, Melanie Schellenberg, Kris Dreher, and Lena Maier-Hein. Deep learning for biomedical photoacoustic imaging: a review. *Photoacoustics*, 22:100241, 2021.
- [19] Changchun Yang, Hengrong Lan, Feng Gao, and Fei Gao. Review of deep learning for photoacoustic imaging. *Photoacoustics*, 21:100215, 2021.
- [20] Stephan Antholzer, Markus Haltmeier, and Johannes Schwab. Deep learning for photoacoustic tomography from sparse data. *Inverse problems in science and engineering*, 27(7):987–1005, 2019.
- [21] Jiasheng Zhou, Da He, Xiaoyu Shang, Zhendong Guo, Sung-Liang Chen, and Jiajia Luo. Photoacoustic microscopy with sparse data by convolutional neural networks. *Photoacoustics*, 22:100242, 2021.
- [22] Steven Guan, Amir A Khan, Siddhartha Sikdar, and Parag V Chitnis. Limited-view and sparse photoacoustic tomography for neuroimaging with deep learning. *Scientific reports*, 10(1):1–12, 2020.
- [23] Huijuan Zhang, LI Hongyu, Nikhila Nyayapathi, Depeng Wang, Alisa Le, Leslie Ying, and Jun Xia. A new deep learning network for mitigating limited-view and under-sampling artifacts in ring-shaped photoacoustic tomography. *Computerized Medical Imaging and Graphics*, 84:101720, 2020.
- [24] Hongming Shan, Christopher Wiedeman, Ge Wang, and Yang Yang. Simultaneous reconstruction of the initial pressure and sound speed in photoacoustic tomography using a deep-learning approach. In *Novel Optical Systems, Methods, and Applications XXII*, volume 11105, page 1110504. International Society for Optics and Photonics, 2019.
- [25] Maarten V. de Hoop, Matti Lassas, and Christopher A. Wong. Deep learning architectures for nonlinear operator functions and nonlinear inverse problems. *Mathematical Statistics and Learning*, no. 1/2(4):1–86, 2021
- [26] Saeed Shurrah and Rehab Duwairi. Self-supervised learning methods and applications in medical imaging analysis: A survey. *PeerJ Computer Science*, 8:e1045, 2022.
- [27] Longlong Jing and Yingli Tian. Self-supervised visual feature learning with deep neural networks: A survey. *IEEE transactions on pattern analysis and machine intelligence*, 43(11):4037–4058, 2020.
- [28] Sunghwan Moon. Inversion formula for a radon-type transform arising in photoacoustic tomography with circular integrating detectors. *Advances in Mathematical Physics*, 2018, 2018.
- [29] Rim Gouia-Zarrad, Souvik Roy, and Sunghwan Moon. Numerical inversion and uniqueness of a spherical radon transform restricted with a fixed angular span. *Applied Mathematics and Computation*, 408:126338, 2021.

- [30] Olaf Ronneberger, Philipp Fischer, and Thomas Brox. U-net: Convolutional networks for biomedical image segmentation. In International Conference on Medical image computing and computer-assisted intervention, pages 234–241. Springer, 2015.
- [31] Wenzhe Shi, Jose Caballero, Ferenc Huszár, Johannes Totz, Andrew P Aitken, Rob Bishop, Daniel Rueckert, and Zehan Wang, Real-time single image and video super-resolution using an efficient sub-pixel convolutional neural network Proceedings of the IEEE conference on computer vision and pattern recognition, 1874–1883, 2016.
- [32] George Cybenko. Approximation by superpositions of a sigmoidal function. Mathematics of control, signals and systems, 2(4):303–314, 1989.
- [33] Jae-Mo Kang and Sunghwan Moon. Error bounds for ReLU networks with depth and width parameters. Japan Journal of Industrial and Applied Mathematics, To appear.
- [34] T Douglas Mast, Laurent P Souriau, D-LD Liu, Makoto Tabei, Adrian I Nachman, and Robert C Waag. A  $k$ -space method for large-scale models of wave propagation in tissue. IEEE transactions on ultrasonics, ferroelectrics, and frequency control, 48(2):341–354, 2001.
- [35] Benjamin T Cox, S Kara, Simon R Arridge, and Paul C Beard.  $k$ -space propagation models for acoustically heterogeneous media: Application to biomedical photoacoustics. The Journal of the Acoustical Society of America, 121(6):3453–3464, 2007.
- [36] Lawrence A Shepp and Benjamin F Logan. The Fourier reconstruction of a head section. IEEE Transactions on nuclear science, 21(3):21–43, 1974.
- [37] Diederik P Kingma and Jimmy Ba. Adam: A method for stochastic optimization. arXiv preprint arXiv:1412.6980, 2014.